Infectious Disease Modelling 9 (2024) 657–672

Contents lists available at ScienceDirect

Infectious Disease Modelling

journal homepage: www.keaipublishing.com/idm

Influence of waning immunity on vaccination decision-making: A multi-strain epidemic model with an evolutionary approach analyzing cost and efficacy

Md. Mamun-Ur-Rashid Khan [a, c, *], Jun Tanimoto [a, b]

[a] Interdisciplinary Graduate School of Engineering Sciences, Kyushu University, Kasuga-koen, Kasuga-shi, Fukuoka, 816-8580, Japan
[b] Faculty of Engineering Sciences, Kyushu University, Kasuga-koen, Kasuga-shi, Fukuoka, 816-8580, Japan
[c] Department of Mathematics, University of Dhaka, Dhaka, 1000, Bangladesh

ARTICLE INFO

Article history:
Received 4 January 2024
Received in revised form 12 March 2024
Accepted 19 March 2024
Available online 24 March 2024
Handling Editor: Dr. Raluca Eftimie

Keywords:
Multistrain epidemic model
Vaccination
Behavior dynamics
Waning immunity
Social dilemma

ABSTRACT

In this research, we introduce a comprehensive epidemiological model that accounts for multiple strains of an infectious disease and two distinct vaccination options. Vaccination stands out as the most effective means to prevent and manage infectious diseases. However, when there are various vaccines available, each with its costs and effectiveness, the decision-making process for individuals becomes paramount. Furthermore, the factor of waning immunity following vaccination also plays a significant role in influencing these choices. To understand how individuals make decisions in the context of multiple strains and waning immunity, we employ a behavioral model, allowing an epidemiological model to be coupled with the dynamics of a decision-making process. Individuals base their choice of vaccination on factors such as the total number of infected individuals and the cost-effectiveness of the vaccine. Our findings indicate that as waning immunity increases, people tend to prioritize vaccines with higher costs and greater efficacy. Moreover, when more contagious strains are present, the equilibrium in vaccine adoption is reached more rapidly. Finally, we delve into the social dilemma inherent in our model by quantifying the social efficiency deficit (SED) under various parameter combinations.

1. Introduction

Vaccination stands as the foremost strategy for preventing infectious diseases. However, the proliferation of diverse vaccines has introduced a conundrum among individuals, creating confusion in the selection process (Buonomo, 2020; Khan et al., 2022a, 2023; Zuo, Zhu, & Ling, 2022). This dilemma is exacerbated in the context of diseases with multiple strains, accentuating the critical nature of informed vaccine selection (Khan et al., 2022a, 2023). The pivotal determinants in this decision-making process revolve around the economic considerations associated with vaccination cost and the efficacy of the chosen vaccine (Ariful Kabir, Jusup, & Tanimoto, 2019; Fenichela et al., 2011; Kabir, Risa, & Tanimoto, 2021; Kabir & Tanimoto,

* Corresponding author. Interdisciplinary Graduate School of Engineering Sciences, Kyushu University, Kasuga-koen, Kasuga-shi, Fukuoka, 816-8580, Japan.
E-mail address: mamun.math@du.ac.bd (Md.M.-U.-R. Khan).
Peer review under responsibility of KeAi Communications Co., Ltd.

https://doi.org/10.1016/j.idm.2024.03.004

2020; Rajib Arefin, Masaki, Ariful Kabir, & Tanimoto, 2019; Tori & Tanimoto, 2022). Despite the established efficacy of vaccination, not all individuals opt for this preventive measure. Some individuals acquire immunity through natural exposure to infectious agents or contribute to the development of natural herd immunity. In specific cases, individuals may favor periodic vaccinations, as exemplified by the seasonal administration of influenza vaccines (Chun-Miin Chen, 2021; Kabir, 2021; Rajib Arefin et al., 2019). Notably, the ongoing COVID-19 pandemic shares resemblances with seasonal influenza, warranting recurrent vaccinations due to the diminishing protective effects over time (Markovič, Šterk, Marhl, Perc, & Gosak, 2021; Nana-kyere et al., 2022; Webb, 2021; Wu, 2021; Zuo, Zhu, & Ling, 2022; Zuo, Zhu, Meng, et al., 2022). Individual choices regarding vaccination are further molded by prevailing infection rates and the financial implications of vaccine acquisition.

In the examination of infectious disease models, compartmental models emerge as the preeminent tool for scientific and healthcare management authorities. The foremost among these models is the SIR model, pioneered by Kermack and McKendrick, delineating the progression of disease in humans through sequential transitions from the susceptible compartment (S) to the infected compartment (I) and ultimately to the recovered compartment (R), where immunity to reinfection develops (Kermack & McKendrick, 1927). The phenomenon of waning immunity, manifesting as relapses in recovered individuals, introduces a nuanced consideration.

Certain epidemics necessitate the incorporation of additional compartments, such as Exposed (E), Quarantine (Q), Hospitalized (H), and Asymptomatic (A), to comprehensively investigate disease dynamics (Buonomo, 2020; Cabrera, Córdova-Lepe, Gutiérrez-Jara, & Vogt-Geisse, 2021; Dong, Xu, Ding, & Bo, 2023; Kabir et al., 2019a, 2019b; Khalaf & Flayyih, 2023; Kumar & Abbas, 2022; Turkyilmazoglu, 2021, 2022a, 2022b; Tyson, Hamilton, Lo, Baumgaertner, & Krone, 2020; Utsumi, Arefin, Tatsukawa, & Tanimoto, 2022; Wang, Liu, Zhang, & Xie, 2023). Furthermore, compartmental models find applicability in exploring disease transmission interventions, including the scrutiny of supervision and moderation methods like immunization, as well as the impact of demographic factors.

While SIR dynamics afford analysis of various elements such as resource exploitation, corruption, and the dissemination of misinformation, it is noteworthy that most models tend to emphasize the pathogenesis of the illness rather than individual behavior within specific circumstances. However, it is pivotal to acknowledge that numerous infectious disease control strategies hinge on organizational and human decision-making processes (Buonomo, 2020; Kabir, Kuga, & Tanimoto, 2020; Khan et al., 2023; Khan & Tanimoto, 2023; Markovič et al., 2021; Turkyilmazoglu, 2022b).

The nascent field of behavioral epidemiology, an amalgamation of game theory and psychology with epidemiology, has gained significant attention in addressing this gap. Behavioral epidemiology diverges from fixed role paradigms, focusing on individual behavior as a key determinant. In this context, sociophysics emerges as a cutting-edge discipline utilizing Evolutionary Game Theory (EGT) and statistical physics to enhance the understanding of human behavior (Kabir, 2021; Kabir et al., 2021; Kabir & Tanimoto, 2020; Khan et al., 2022a, 2022b, 2023; Khan & Tanimoto, 2023; Tanimoto, 2015, 2021).

An innovative approach, as exemplified by Bauch (Bauch, 2005), involves the integration of the SIR model with EGT to scrutinize the dynamics of vaccine decision-making. By considering disease dynamics, total infected individuals, infection cost, vaccination cost, and vaccine efficacy, this approach facilitates personalized vaccination decisions, culminating in the concept of the "vaccination game". The application of this method has yielded numerous insights and predictions pertinent to vaccination campaigns (Kabir, 2021; Kabir et al., 2019b, 2020; Nishimura, Arefin, Tatsukawa, & Utsumi, 2023; Rajib Arefin et al., 2019).

Aside from the standpoint of epidemiological modeling, the question of how people adopt a vaccine; whether willing to commit or to avoid it, and which vaccine is favored amid several alternatives, is important. It should be said still a difficult problem to reproduce in a mathematical model, although some field survey studies were explored (e.g. (Kabir, Ovi, Murtyas, Hagishima, & Tanimoto, 2023)).

In this investigation, we present a comprehensive behavioral epidemic model featuring multiple strains, built upon the SIRS/V dynamics and incorporating two distinct vaccination options. Our model allows individuals to make vaccination choices based on key factors such as the total number of infected individuals, vaccination costs, and the efficacy of available vaccines with the presence of wanning immunity (Chun-Miin Chen, 2021; Fahdilla, Putri, & Haripamyu, 2021; Hamami, Cameron, Pollock, & Shankland, 2017; Nakata & Omori, 2015; Nishimura et al., 2023; Van Boven, De Melker, Schellekens, & Kretzschmar, 2000). The multistrain context enables an exploration of how these behavioral dynamics influence the dominance or coexistence of the two vaccination options over time (Khan et al., 2022a, 2023; Rajib Arefin et al., 2019).

Through the selection of critical parameters within our proposed model, we have computed the fractions of vaccinated individuals at equilibrium, providing insights into the emergence of vaccine dominance. The behavioral model serves as a framework for guiding individual vaccination strategies.

To delve into the societal implications of our model, particularly addressing the social dilemma, we utilize essential metrics such as the basic reproduction number, waning rate of immunity, vaccination cost, inertial effect of vaccination rate, and the sensitivity of vaccination choice to cost. Specifically, we quantify the Social Efficiency Deficit (SED), representing the disparity between payoffs at the Nash Equilibrium (NE) and the Social Optimum (SO). This analysis sheds light on the societal consequences of individual vaccination decisions, offering a nuanced understanding of the interplay between individual choices and collective outcomes (Arefin, Kabir, Jusup, Ito, & Tanimoto, 2020; Ariful Kabir et al., 2019; Cabrera et al., 2021; Kabir, 2021; Kabir et al., 2020, 2021; Kabir & Tanimoto, 2019; Khan et al., 2023; Khan & Tanimoto, 2023; Tori & Tanimoto, 2022; Turkyilmazoglu, 2022b; Wei, Lin, & Wu, 2019; Wu, 2021).

2. Model depiction

2.1. Epidemic model

We considered an epidemiological model that consists of two vaccination compartments and n infected compartments with the presence of n strain. All the people are considered Susceptible and initially belong to compartment S. Vaccination compartment V_1 contains those individuals who choose vaccine 1 which has a high cost and high efficacy while V_2 contains those individuals who choose vaccine 2 which is less costly and less efficacy. All the individuals will recover from strain and move to the recovered or removed compartment R. Recovered individuals can be susceptible again with the loss of immunity. The transmission rate from the susceptible compartment is $\beta_i(\beta_i < \beta_{i+1})$, where i starts from 1 to n. We consider both vaccinations imperfect so both individuals from the compartment V_1 and V_2 can be infected with any strain. e_{1i} and e_{2i} are vaccine efficacy of vaccines 1 and 2. Here, the efficacy obeys the concept of effectiveness (Kuga & Tanimoto, 2018). So the discounted transmission rates from vaccine 1 and vaccine 2 compartments will be $(1-e_{1i})\beta_i$ and $(1-e_{2i})\beta_i$ respectively. We define the efficacy ratio $e_r = \frac{e_{1i}}{e_{2i}}$ for the two vaccines for n strains to analyze the dynamics of vaccination. The recovery rates for n strains are γ_i. In addition, we considered $\gamma_i < \gamma_{i+1}$ to keep the basic reproduction number at a fixed value which makes the model simpler. With the rate ω, individuals become susceptible again which we call the waning immunity. The schematic diagram of the proposed model is shown in Fig. 1 and the set of Ordinary differential equations is as follows:

$$\dot{S} = -xS - yS - \sum_{i=1}^{n} \beta_i S I_i + \omega R, \tag{1}$$

$$\dot{V_1} = xS - \sum_{i=1}^{n} (1-e_{1i})\beta_i V_1 I_i, \tag{2}$$

$$\dot{V_2} = yS - \sum_{i=1}^{n} (1-e_{2i})\beta_i V_2 I_i, \tag{3}$$

$$\left.\begin{aligned} \dot{I_1} &= (1\text{-}e_{11})\beta_1 V_1 I_1 + \beta_1 S I_1 + (1\text{-}e_{21})\beta_1 V_2 I_1 - \gamma_1 I_1, \\ \dot{I_2} &= (1\text{-}e_{12})\beta_2 V_1 I_2 + \beta_2 S I_2 + (1\text{-}e_{22})\beta_2 V_2 I_2 - \gamma_2 I_2, \\ &\cdots\cdots\cdots \\ \dot{I_n} &= (1\text{-}e_{1n})\beta_n V_1 I_n + \beta_n S I_n + (1\text{-}e_{2n})\beta_n V_2 I_n - \gamma_n I_n, \end{aligned}\right\} \tag{4}$$

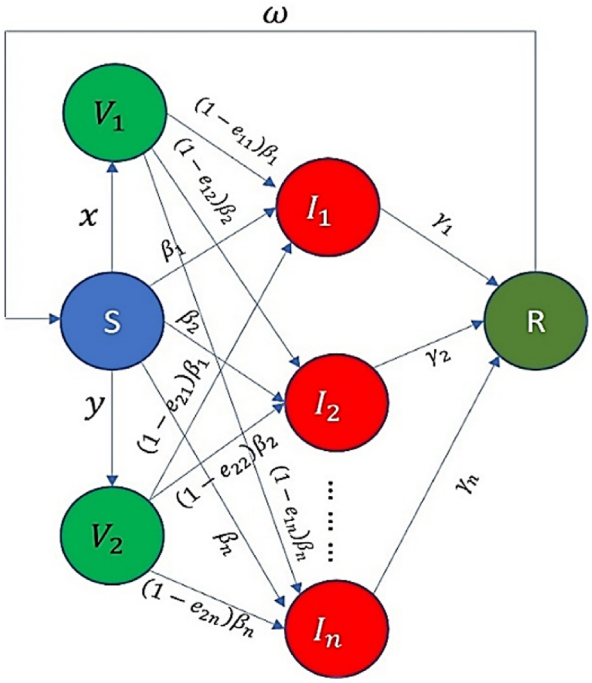

Fig. 1. The compartments and their transition of the proposed model.

$$\dot{R} = \sum_{i=1}^{n} \gamma_i I_i - \omega R, \tag{5}$$

$$S(t) + V_1(t) + V_2(t) + \sum_{i=1}^{n} I_i(t) + R(t) = 1, \tag{6}$$

2.2. Behavior model

For the vaccination flux from the susceptible to vaccination compartments, we considered the famous behavior model originated by Bauch (Bauch, 2005). At rates x and y susceptible individuals can choose their vaccine 1 and vaccine 2 respectively. We define the dynamical equations:

$$\dot{x} = m\,x\,(1-x)\left\{ c\sum_{i=1}^{n} I_i - kc_{v1} \right\}, \tag{7}$$

$$\dot{y} = m\,y\,(1-y)\left\{ c\sum_{i=1}^{n} I_i - kc_{v2} \right\}, \tag{8}$$

where m is the inertial effect constant and k is the relative sensitivity to the vaccination cost. We considered the values of m and k will be equal to keep the general tendency for two vaccinations equal. c_{v1} and c_{v2} are the vaccination cost of vaccines 1 and 2 respectively where we consider that the cost of vaccine 1 is up to 1 and always greater or equal to the cost of vaccine 2 (i.e.,$0 \le c_{v1} \le 1$ and $0 \le c_{v2} \le c_{v1}$). c is the cost of disease that should be paid by every infected individual and we consider that the value of c is 1 throughout our work (i.e.,$c = 1$). With the increase in the value of the summation i.e., the total number of infected individuals at any time t with all strains the above equations always increase the values of x and y i.e., the vaccination uptake while increasing the cost of the vaccinations always reduces the vaccination uptake.

2.3. Basic reproduction number, vaccine equilibrium, fraction of vaccinated individuals, total vaccination, total infection, average social payoff (ASP), social efficiency deficit (SED)

In this model, we considered the standard value of the basic reproduction number, $R_0 = \frac{\beta_i}{\gamma_i} = 2.5$ (Bauch, 2005). However, in the latter segment of the discussion of the results, we also examined the interplay between vaccination behavior and disease dynamics across various values of the basic reproduction number.

To get the vaccine equilibrium we need to set equations (7) and (8) equal to zero. i.e.,

$$\dot{x} = m\,x\,(1-x)\left\{ c\sum_{i=1}^{n} I_i - kc_{v1} \right\} = 0$$

$$\dot{y} = m\,y\,(1-y)\left\{ c\sum_{i=1}^{n} I_i - kc_{v2} \right\} = 0$$

Since, $m, x, c\sum_{i=1}^{n} I_i - kc_{v1}$ cannot be zero because $m = 0$ or $x = 0$ implies constant or no vaccination flow and $c\sum_{i=1}^{n} I_i$ is also nonzero, the only possibility is $(1-x) = 0$ which implies $x = 1$.

Similarly, we can get $y = 1$.

So the equilibrium point for the vaccination is $(x,y) = (1,1)$. This is assuming I_i are nonzero, k is positive and the conditions between c_{v1} and c_{v2} ($0 \le c_{v1} \le 1$ and $0 \le c_{v2} \le c_{v1}$) are satisfied.

The fractions of vaccinated individuals for both vaccinations are defined as follows:

$$V_1R = \frac{V_1(\infty)}{V_1(\infty) + V_2(\infty)}, \tag{9}$$

$$V_2R = \frac{V_2(\infty)}{V_1(\infty) + V_2(\infty)}, \tag{10}$$

where $t = \infty$ denotes a state of equilibrium or steady state (we say it, Nash equilibrium NE).

The total number of vaccinated individuals from vaccination 1, and vaccination 2 are defined as follows:

$$V_1T = \int_0^\infty (xS)\, dt, \tag{11}$$

$$V_2T = \int_0^\infty (yS)\, dt, \tag{12}$$

$$VT = V_1T + V_2T, \tag{13}$$

The total number of infected individuals from vaccination 1, vaccination 2, and susceptible are defined as:

$$IV_1T = \int_0^\infty \left(\sum_{i=1}^{n} \beta_i (1 - e_{1i}) I_i V_1 \right) dt, \tag{14}$$

$$IV_2T = \int_0^\infty \left(\sum_{i=1}^{n} \beta_i (1 - e_{2i}) I_i V_2 \right) dt, \tag{15}$$

$$IST = \int_0^\infty \left(\sum_{i=1}^{n} \beta_i I_i S \right) dt, \tag{16}$$

$$IT = IV_1T + IV_2T + IST, \tag{17}$$

where $t = \infty$ denotes a state of equilibrium or steady state (we say it, Nash equilibrium NE).

The ASP at NE is defined as follows:

$$ASP_{NE} = -IT^*c - V_1T^*c_{v1} - V_2T^*c_{v2}, \tag{18}$$

where the first term on the right-hand side indicates the total payoff due to infection and the second and third terms indicate the payoffs of the individuals who commit vaccination 1 and vaccination 2 respectively.

By referencing the original definition of the Social Efficiency Deficit (SED), we assess the disparity between the Average System Payoff (ASP) at the Nash Equilibrium (NE) and the ASP at the Social Optimum (SO), thereby discerning the potential existence of a social dilemma within the present social-dynamical system (ASP_{SO}). This analysis elucidates the means to enhance the system's ASP, transitioning from an evolutionarily stable state (NE) to a theoretically optimal societal state, maximizing the attainable ASP_{SO} when all evolutionary processes represented by variables x and y are effectively managed (Arefin et al., 2020).

It is defined as follows:

$$SED = ASP_{SO} - ASP_{NE}, \tag{19}$$

The SO state is a time-constant vector $(x\ (for\ SO), y\ (for\ SO))$, with x, y ranging in $[0, 1]$. Thus,

$$\boldsymbol{SO} = \arg\ \max\ [ASP(x\ (for\ SO), y\ (for\ SO))]. \tag{20}$$

When NE equals SO, SED implies zero. However, when the SED is positive but not zero, there is a social dilemma.

3. Results and discussion

3.1. Impact of waning immunity ω on vaccination choice

In this section, we present time series data for compartments V_1 and V_2, with a focus on analyzing the impact of waning immunity in the context of vaccination choices. The figures herein are generated using the established set of parameter values outlined in Table 2. Furthermore, Table 3 provides the initial values for each compartment and the associated flow rates. Within this framework, we examine various scenarios denoted by the parameter $"n"$ which can take on values of 2, 3, and 4, corresponding to models featuring two, three, and four viral strains, respectively. As previously noted, these newer strains are characterized by higher transmission rates in comparison to their predecessors. In Fig. 2 (a) – (c), we illustrate the vaccination compartments under the assumption of waning immunity ($\omega = 0.05$) for two, three, and four strains, respectively. The time series spans 3000 days. Across all cases in Fig. 2(a)– (c), it is evident that individuals consistently favor the second vaccine option, characterized by lower cost and reduced efficacy. Fig. 2(d)– (f) provide insights into the flow rates from susceptible individuals to vaccinated compartments, serving as a complementary visual representation to Fig. 2(a)– (c). These figures

Table 1
Description of the model parameters.

Parameter symbol	Parameter Description
β_i	Disease Transference rate due to strain i
γ_i	The recovery rate from strain i
e_{1i}	The efficacy of the vaccine 1 to strain i
e_{2i}	The efficacy of the vaccine 2 to strain i
e_r	Efficacy ratio
m	Inertial effect on migration from S to V_1 and S to V_2
k	Sensitivity to vaccination due to cost
c	Disease cost
c_{v1}	Cost of the vaccine 1
c_{v2}	Cost of the vaccine 2
ω	Waning rate against immunity

Table 2
Standard values of the parameters (Khan et al., 2022a, 2023; Tatsukawa et al., 2021, 2022; Utsumi et al., 2022).

Parameter	Value	Parameter	Value	Parameter	Value	Parameter	Value
β_1	0.4	γ_1	0.16	e_{11}	0.9	e_{21}	0.6
β_2	0.6	γ_2	0.24	e_{12}	0.6	e_{22}	0.4
β_3	0.8	γ_3	0.32	e_{13}	0.3	e_{23}	0.2
β_4	1.0	γ_4	0.4	e_{14}	0.2	e_{24}	0.13
m	1.0	k	0.1	e_r	2/3	c	1.0
c_{v1}	0.5	c_{v2}	0.25	ω	0.1		

Table 3
Initial values for the compartments and migration rates (Khan et al., 2022a, 2023; Tatsukawa et al., 2021, 2022; Utsumi et al., 2022).

State	At $\boldsymbol{t} = \mathbf{0}$	State/Rate	At $\boldsymbol{t} = \mathbf{0}$
S	0.994	R	0.00
V_1	0.001	x	0.01
V_2	0.001	y	0.01
I_i $(i = \overline{1,4})$	0.001		

reveal that the transition to compartment V_2 occurs more rapidly, approaching equilibrium and reaching values close to 1 before the transition to V_1. This suggests that susceptible individuals are more inclined to choose a vaccine V_2 over vaccine V_1.

Fig. 3(g) – (h) present time series data for compartments V_1 and V_2, considering two, three, and four strains, all under the assumption of waning immunity with a parameter value of $\omega = 0.1$. Within each panel, we observe a noteworthy phenomenon where Vaccine 1 eventually supersedes Vaccine 2 over time. Furthermore, the increasing number of strains characterized by higher transmission rates leads to an earlier preference for Vaccine 1 among individuals. Fig. 3(j)– (l) display a comparative analysis of flow rates. In each case, the rates eventually converge to an equilibrium state $(x = 1, y = 1)$, with the number of strains showing a positive correlation with the speed at which equilibrium is reached.

Fig. 4(m) – (n) provide a detailed analysis of time series data for compartments V_1 and V_2, taking into account two, three, and four viral strains while incorporating a waning immunity parameter of $\omega = 0.2$. In each of these panels, a consistent trend emerges where Vaccine 1 eventually surpasses Vaccine 2, underscoring the temporal dynamics. Furthermore, as the number of strains increases, each characterized by higher transmission rates, Vaccine 1 establishes its preference among individuals at an earlier stage. Fig. 4(p) – (r) present a comparative examination of flow rates. In each scenario, these rates gradually approach equilibrium $(x = 1, y = 1)$, and once again, we observe that the introduction of a greater number of strains leads to an accelerated attainment of equilibrium, mirroring the pattern observed in the previous case.

3.2. Comparison between the fraction of vaccinated individuals at equilibrium

In the preceding section, we presented outcomes based on the consideration of 2, 3, and 4 strains. Remarkably, our findings indicated a consistent trend when utilizing more than two strains. Consequently, for the subsequent sections of the results, we exclusively employed a 4 – strain configuration to conduct a comprehensive analysis of the remaining outcomes.

In this section, we delve into an examination of the equilibrium fractions of vaccinated individuals, as described by equations (9) and (10), while varying key parameters. Fig. 5 visually represents the proportion of individuals at equilibrium who have chosen vaccine 1. In panels (a) – (d), we construct heatmaps by varying the values of R_0 (ranging from 0.1 to 5.1) along the $y-$ axis and ω (ranging from 0.0 to 0.5) along the $x-$ axis. Additionally, we introduce four distinct values of the efficacy ratio e_r (specifically, $\frac{1}{5}, \frac{1}{3}, \frac{2}{3},$ and 1) to analyze the dominance dynamics between vaccine 1 and vaccine 2. All other parameters are maintained at their standard values as outlined in Table 1.

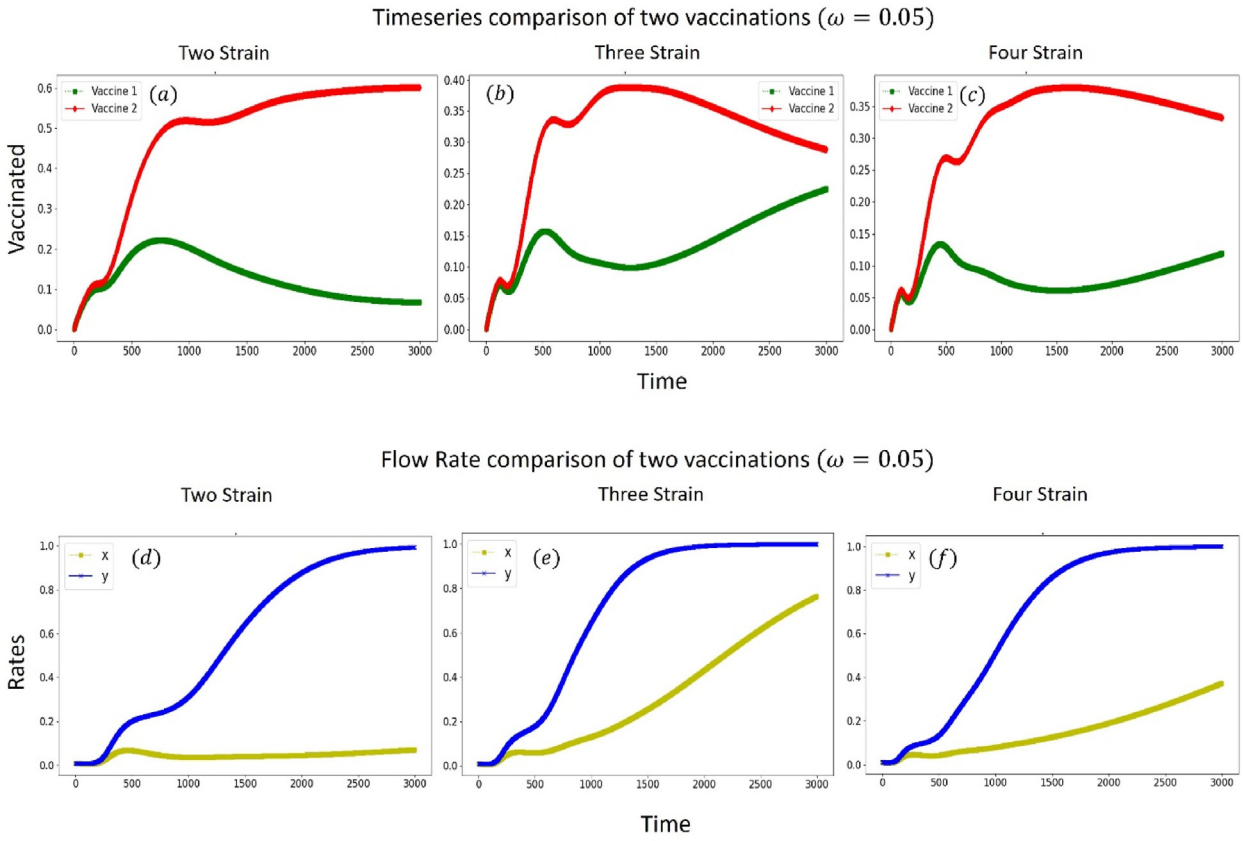

Fig. 2. In the temporal evolution of the vaccination dynamics concerning two, three, and four strains with a specified value of $\omega = 0.05$, the standard parameters remain unchanged. Panels (a) – (c) illustrate timeseries data for the number of vaccinated individuals at time t, with the red curves denoting those who opted for vaccine 2 and the green curves representing individuals who selected vaccine 1. Across all scenarios, it is evident that Vaccine 2 consistently dominates throughout the entire temporal span. Moving on to panels (d) – (f), the focus shifts to the vaccination rates. Here, the observation reveals a consistent dominance of y (Vaccine 2) until the mentioned period ($T = 3000$ days). Throughout this period, y maintains superiority in the vaccination rates over other options. In summary, the visual representation of the timeseries data underscores the persistent dominance of Vaccine 2 in terms of both the number of vaccinated individuals and the vaccination rates, irrespective of the varying number of strains considered, with ω held constant at 0.05.

Across every panel (a) – (d), we discern three distinct regions. The upper right region gradually transitions from red to white as e_r increases. According to the definition in EGT, these regions indicate predominance by vaccine 1, except for panel (d), where light red hues suggest that the value of V_1R is slightly more than 0.5. In panel (d), we can infer that when e_r is close to 1, both vaccines hold an equal priority (coexistence) among individuals due to their identical efficacy. In cases where R_0 and ω are substantial, the choice of vaccination is not significantly affected, provided the efficacies of the vaccines remain equal.

Conversely, the bottom light blue regions and the dark blue regions in the middle signify predominance and dominance by vaccine 2 respectively. When R_0 falls below 1, it indicates that the disease is unlikely to spread extensively, leading individuals to opt for the more cost-effective vaccine. Efficacy holds little sway over vaccination behavior when the disease's transmission is limited. However, as R_0 surpasses 1 and ω increases, individuals tend to select the less expensive vaccine until a certain threshold is reached. Beyond this point, individuals opt for the vaccine with higher efficacy, despite the higher cost.

Fig. 6 presents a depiction of the equilibrium fractions of individuals who have opted for vaccine 1. In panels (a) – (d), we construct heatmaps by varying the cost of vaccine 1 (c_{v1}) within the range of 0.0–1.0 along the $y-$ axis and the cost of vaccine 2 (c_{v2}) within the range of 0.0 to c_{v1} along the $x-$ axis. Moreover, we consider four distinct values of the efficacy ratio (e_r) - specifically, $\frac{1}{5}, \frac{1}{3}, \frac{2}{3}$, and 1 to analyze the dominance dynamics between vaccine 1 and vaccine 2. All other parameters are maintained at their standard values as specified in Table 1.

Across each panel (a) – (d), we observe two primary regions. The upper region gradually transitions from light to dark blue as e_r increases, predominance of vaccine 2 becomes dominant. When e_r is close to 1, individuals tend to opt for vaccine 2, which is the more cost-effective choice.

Conversely, the lower light red regions in every panel, except for panel (d), indicate the predominance of vaccine 1. In panel (d), these regions become white, signifying a coexistence of the two vaccines. Hence, when the cost of vaccine 1 becomes

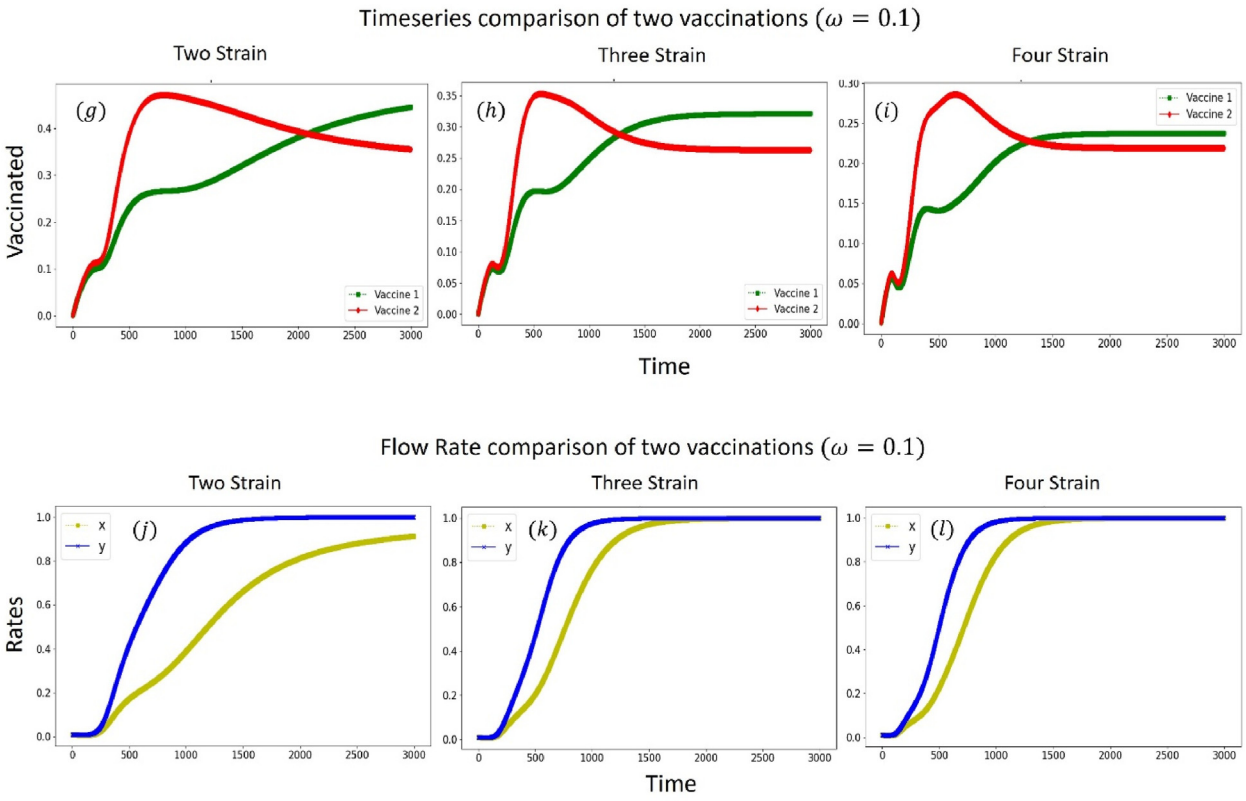

Fig. 3. In the context of a specified value of $\omega = 0.1$, and with the standard parameters remaining unchanged, we examine the timeseries of vaccination compartments and rates for two, three, and four strains. Panels (g) – (i) display the number of vaccinated individuals at time t, with the red curves indicating those who opted for vaccine 2 and the green curves representing individuals who chose vaccine 1. Notably, in each scenario, a discernible shift occurs, and after a certain duration, Vaccine 1 emerges as the dominant choice. This shift in dominance is particularly pronounced in the presence of highly transmissible multiple strains, resulting in an earlier attainment of vaccine equilibrium. Turning attention to panels (j) – (l), which illustrate the vaccination rates, it is observed that both x and y reach equilibrium point 1 after a certain duration. This indicates that, despite initial variations, both vaccines eventually stabilize at the same equilibrium point over time. In summary, the timeseries analysis underscores the dynamic nature of vaccine dominance, with Vaccine 1 emerging as the dominant choice after a certain period. Additionally, the impact of highly transmissible multiple strains is evident in the accelerated arrival of the vaccine equilibrium. In terms of vaccination rates, both x and y eventually converge to equilibrium point 1, demonstrating a stabilization of the system over time.

significantly higher, approaching the cost of managing the disease (c), individuals tend to prefer vaccine 2, regardless of whether the efficacies of the vaccines are equal or unequal.

Fig. 7 presents an analysis of the equilibrium fractions of individuals who have chosen vaccine 1. In panels (a) – (d), we construct heatmaps by varying the parameter m within the range of 0.0–1.0 along the $y-$ axis and the parameter k within the range of 0.0–1.0 along the $x-$ axis. Additionally, we consider four distinct values of the efficacy ratio (e_r), specifically, $\frac{1}{5}, \frac{1}{3}, \frac{2}{3}$, and 1 to examine the dynamics of dominance between vaccine 1 and vaccine 2. All other parameters remain set at their standard values as specified in Table 1.

Across every panel (a) – (d), we observe three distinct regions. In panels (a)– (c), the left region is predominated by vaccine 1, while in panel (d), the left region becomes coexistent. As the efficacy ratio increases, there is a transition from vaccine 1 dominance to coexistence. This shift occurs because, in scenarios characterized by low sensitivity and a high level of inertial effect, individuals tend to prefer the vaccine with a higher cost. Conversely, higher relative sensitivity leads to the emergence of dark blue regions in every panel, where vaccine 2 becomes the dominant choice. In essence, high sensitivity implies a preference for the less expensive vaccination option.

Of particular interest are the regions in panels (a) – (c) and the third region, which disappears in panel (d), located in the upper right corner with dark red hues. In this region, vaccine 1 dominates, primarily due to the substantial increase in the inertial effect, leading to a heightened flow of vaccination, particularly with a high cost. However, this region diminishes as the efficacy ratio increases. In other words, when efficacy becomes equal, cost takes precedence in the choice of vaccination, favoring vaccine 2.

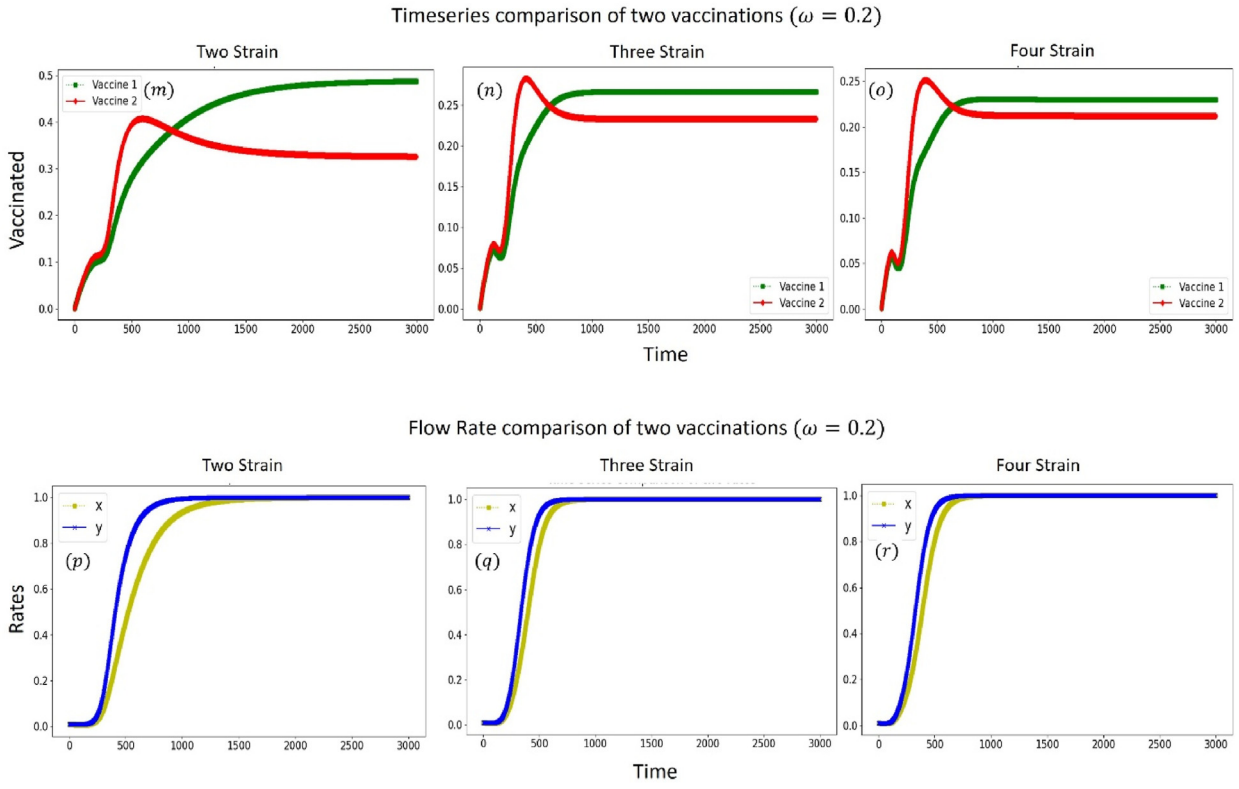

Fig. 4. Temporal profiles of vaccination compartments and rates are examined for two, three, and four strains with ω held constant at 0.2, while the remaining parameters adhere to the standard configuration. In panels (m) – (o), the red curves delineate the count of individuals vaccinated at time t who selected vaccine 2, while the green curves represent those who chose vaccine 1. Notably, in each scenario, there is a discernible temporal pattern where Vaccine 1 attains dominance after a specific duration. The concurrent presence of highly transmissible multiple strains expedites the establishment of vaccine equilibrium. Turning attention to panels (p)– (r), which depict vaccination rates, it is observed that both x and y converge to equilibrium point 1 after a certain duration. In contrast to the findings in Fig. 3, a notable observation is a the earlier dominance of vaccine 1 in every scenario. In summary, the analysis of the timeseries data underscores the temporal dynamics of vaccine dominance and equilibrium, particularly accentuated by the presence of highly transmissible multiple strains. The acceleration of the dominance of vaccine 1 is a notable departure from the observations in Fig. 3.

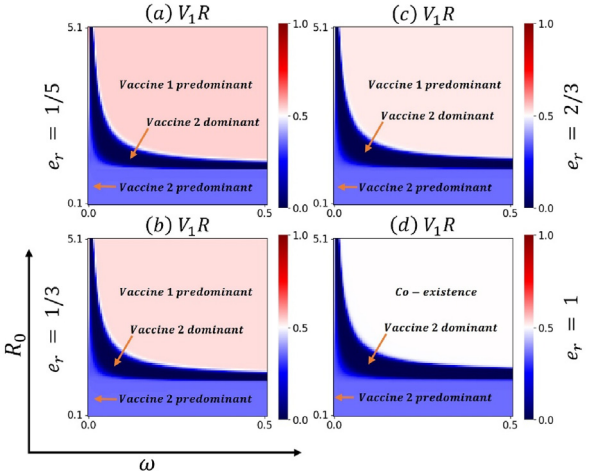

Fig. 5. Heatmaps are employed as a visual tool to illustrate the proportion of individuals who have selected vaccine 1 at equilibrium. Panels (a) – (d) showcase four distinct heatmaps, each corresponding to different efficacy ratio values (e_r) of $\frac{1}{5}, \frac{1}{3}, \frac{2}{3}$, and 1. The spatial orientation is delineated by the waning immunity rate (ω) along the x-axis, ranging from 0 to 0.5, and the basic reproduction number (R_0) along the y-axis, ranging from 0.1 to 5.1. The color gradient on the heatmap scale varies from 0 to 1, with blue denoting the prevalence of vaccine 2, red indicating the dominance of vaccine 1, and white representing the co-existence of both vaccines.

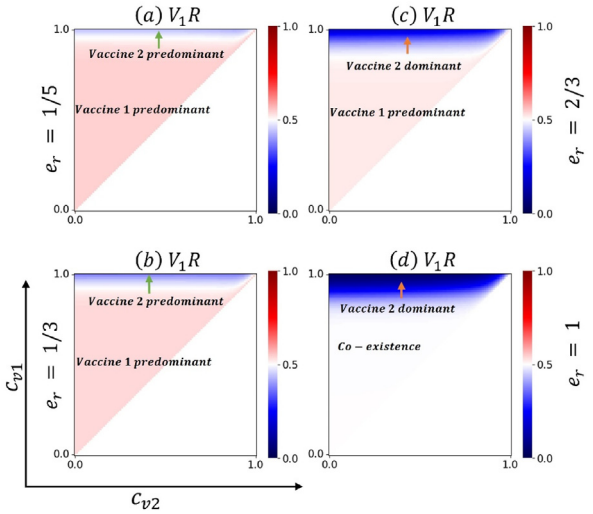

Fig. 6. Heatmaps are utilized to visualize the proportion of individuals who have opted for vaccine 1 at equilibrium. Panels (a) – (d) present four distinct heatmaps corresponding to efficacy ratio values (e_r) of $\frac{1}{5}, \frac{1}{3}, \frac{2}{3}$, and 1. All the panels are drawn in terms of the cost of vaccine 1 (c_{v1}) along the y-axis ranging from 0 to 1 and the cost of vaccine 2 (c_{v2}) along the x- axis both ranging from 0 to c_{v1}. The color gradient on the heatmap scale ranges from 0 to 1, where blue indicates the dominance of vaccine 2, red signifies the dominance of vaccine 1, and white denotes the co-existence of both vaccines. Note that there is almost no sensitivity from c_{v2}. It is conceivable just because vaccines 1 or 2 give predominant results from the ratio of those two vaccine costs, not absolute values.

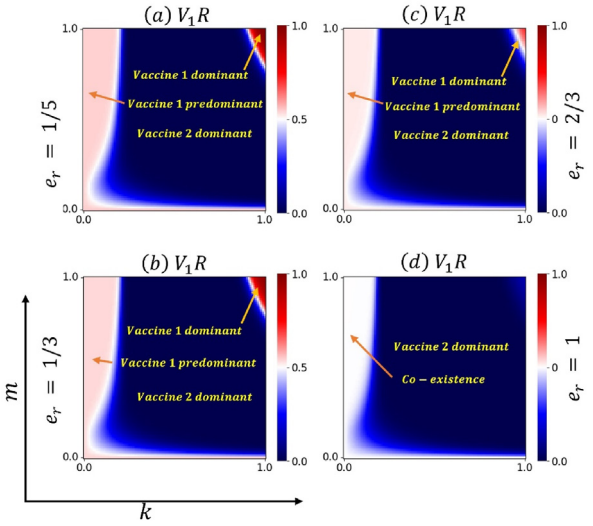

Fig. 7. Heatmaps serve as a visual aid to depict the proportion of individuals choosing vaccine 1 at equilibrium. Panels (a) – (d) present four distinct heatmaps, each corresponding to various efficacy ratio values (e_r) of $\frac{1}{5}, \frac{1}{3}, \frac{2}{3}$, and 1. The spatial arrangement is determined by the impact of sensitivity to vaccination cost (k) along the x-axis, ranging from 0 to 1.0, and the influence of the inertial effect of vaccination rate (m) along the y-axis, ranging from 0.0 to 1.0. The color spectrum on the heatmap scale ranges from 0 to 1, where blue indicates the predominance of vaccine 2, red signals the dominance of vaccine 1, and white signifies the co-existence of both vaccines.

3.3. Analysis of average social payoff (ASP) and social efficiency deficit (SED)

3.3.1. ASP and SED in terms of basic reproduction number and waning immunity

The top row of Fig. 8 provides an overview of key metrics for the NE state, including the total number of vaccinated individuals, the total number of infected individuals, and the Average Social Payoff (ASP). The second row focuses on the SO state, featuring the total number of vaccinated individuals, the total number of infected individuals, the ASP, and the Social Efficiency Deficit (SED). All panels are presented in terms of the waning immunity rate (ω) along the $x-$ axis (ranging from 0.0 to 0.5) and the Basic Reproduction Number (R_0) along the $y-$ axis (ranging from 0.1 to 5.1).

In panel (a), when R_0 is less than 1, the number of vaccinated individuals remains very low. Similarly, in panel (b), if R_0 is less than 1, the number of infected individuals is minimal. Combining these factors and considering their associated costs in

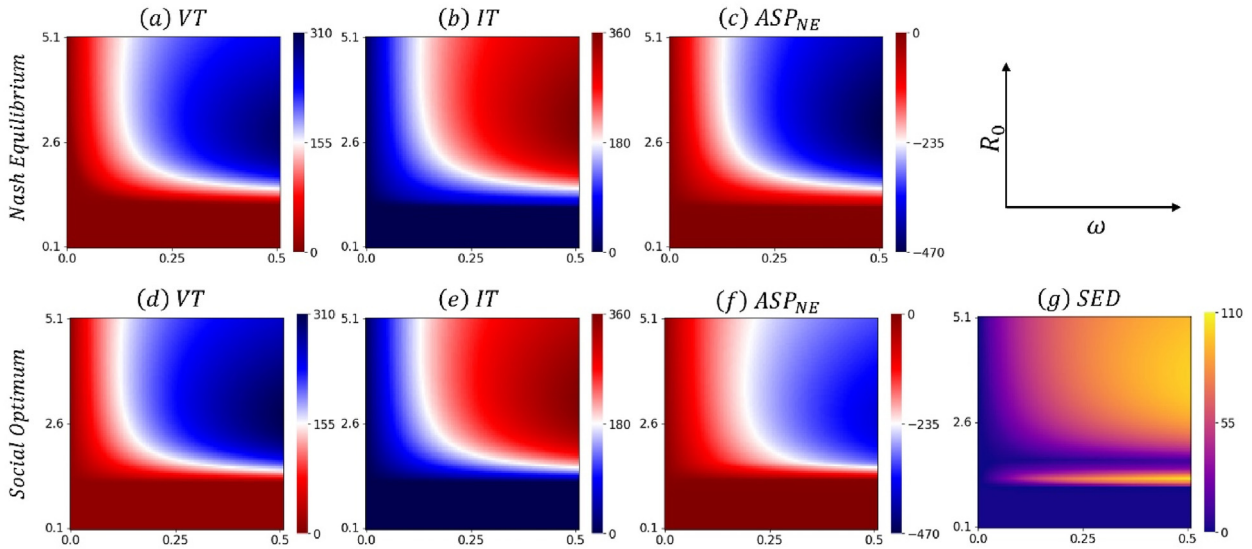

Fig. 8. The total number of vaccinated people, the total number of infected people, ASP, and SED. Panels (a) – (c) are for the NE case and panels (d) – (f) are for the SO case. Panel (g) represents the SED, which is the difference between panels (f) and (c). All the panels are drawn in terms of the waning immunity rate (ω) along the $x-$ axis ranging from 0 to 0.5 and the basic reproduction number (R_0) along the $y-$ axis both ranging from 0.1 to 5.1 The total number of vaccinated people is depicted with a range from 0 to 310, the total number of infected people is depicted with a range from 0 to 360, the ASPs are depicted with a range from – 470 to 0 and the SED is depicted with a range from 0 to 110. The other parameters are the same as in the basic case. From the figures, we see that the social dilemma appears just after R_0 crosses 1 and decreases for a while and then again monotonically increasing with the increase in both waning immunity rate and basic reproduction number. The dilemma will be maximum if both R_0 and ω is maximum.

panel (c), the ASP is also low when R_0 is less than 1. This aligns with the understanding that an R_0 less than 1 implies limited disease spread, resulting in low vaccination and infection rates, consequently yielding a low ASP.

As R_0 surpasses 1, all panels (a) – (c) demonstrate a monotonic increase in the number of vaccinated and infected individuals as both R_0 and ω increase. Consequently, the ASP exhibits a corresponding monotonic increase.

Panels (d) – (f) illustrate the social optimum cases, showcasing a similar trend to panels (a)– (c) but with relatively lower values. Panel (g), depicting the Social Efficiency Deficit (SED), highlights distinctive regions. When the basic reproduction number (R_0) is below 1 (indicated by the dark purple region), and the disease does not propagate significantly, resulting in an absence of an actual social dilemma regarding vaccination. Subsequently, a yellow region emerges with an elevation in R_0, signifying the onset of disease spread. This phase represents a transient state from a disease-free condition to a diseased state. In the presence of multiple vaccines, individuals face heightened uncertainty regarding the decision to undergo vaccination and the selection of the most beneficial vaccine. Following this transitional phase, a conventional scenario unfolds when R_0 surpasses 1. In this case, the disease becomes established, prompting individuals to opt for vaccination and reducing the social dilemma, as indicated by the purple region. Moreover, as both R_0 and the waning immunity rate (ω) increase, the social dilemma exhibits a monotonic escalation, transitioning from purple to yellow regions. The social dilemma attains its maximum magnitude when both R_0 and ω reach their peak values.

The top row of Fig. 9 provides a comprehensive overview of crucial metrics for the NE state, including the total number of vaccinated individuals, the total number of infected individuals, and the Average Social Payoff (ASP). The second row focuses on the SO state, featuring the total number of vaccinated individuals, the total number of infected individuals, the ASP, and the SED. Each panel is delineated by the cost of vaccine 1 (c_{v1}) along the $y-$ axis (ranging from 0 to 1) and the cost of vaccine 2 (c_{v2}) along the $x-$ axis (ranging from 0 to c_{v1}).

In panel (a), the total number of vaccinated individuals reaches a minimum when both vaccine costs are maximized, a scenario that aligns with expectations. As the cost of vaccine 1 increases significantly, panel (b) illustrates a corresponding increase in the total number of infected individuals.

Panel (c) depicts the ASP, considering the total number of infected and vaccinated individuals multiplied by their associated costs. Notably, an increase in vaccination costs leads to a rise in the total average social payoff.

In the social optimum (SO) panels (d) – (f), the suggested strategy is to maximize the number of vaccinated individuals, minimize the number of infected individuals, and consequently, minimize the ASP respectively. The difference between panel (f) and panel (c) is represented in panel (g), illustrating the SED. In the SED panel, it is evident that an increase in both vaccine costs exacerbates the social dilemma, reaching its maximum when both costs are at their highest levels.

A detailed analysis of the most important metrics for the NE state is shown in the upper row of Fig. 10. These metrics include the total number of vaccinated persons, the total number of infected individuals, and the Average Social Payoff (ASP). The second row focuses on the SO state, featuring the total number of vaccinated individuals, the total number of infected

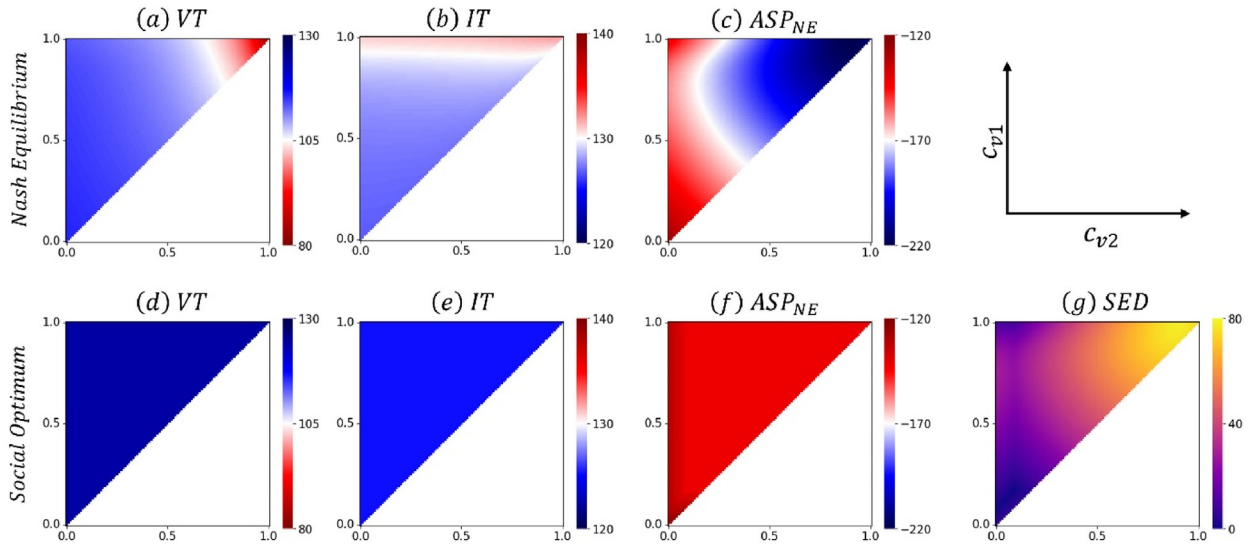

Fig. 9. The total number of vaccinated people, the total number of infected people, ASP, and SED. Panels (a) – (c) are for the NE case and panels (d) – (f) are for the SO case. Panel (g) represents the SED, which is the difference between panels (f) and (c). All the panels are drawn in terms of the cost of vaccine 1 (c_{v1}) along the $y-$ axis ranging from 0 to 1 and the cost of vaccine 2 (c_{v2}) along the $x-$ axis both ranging from 0 to c_{v1}. The total number of vaccinated people is depicted with a range from 0 to 130, the total number of infected people is depicted with a range from 0 to 140, the ASPs are depicted with a range from – 220 to – 120 and the SED is depicted with a range from 0 to 80. The other parameters are the same as in the basic case. From the figures, we see that the social dilemma is maximum when both the cost is maximum.

individuals, the ASP, and the SED. Each panel is delineated by the inertial effect of vaccination (m) along the $y-$ axis (ranging from 0 to 1) and the sensitivity parameter (k) along the $x-$ axis (ranging from 0 to 1).

In panels (a) – (b), an observable trend emerges, indicating that an increase in the inertial effect (m) and a decrease in the sensitivity parameter (k) correspond to an increase in vaccination uptake and a decrease in the number of infected individuals. This alignment is plausible, as a higher inertial effect tends to boost vaccination uptake, while lower sensitivity to cost reduces vaccination uptake. The impact on infected individuals follows a similar pattern.

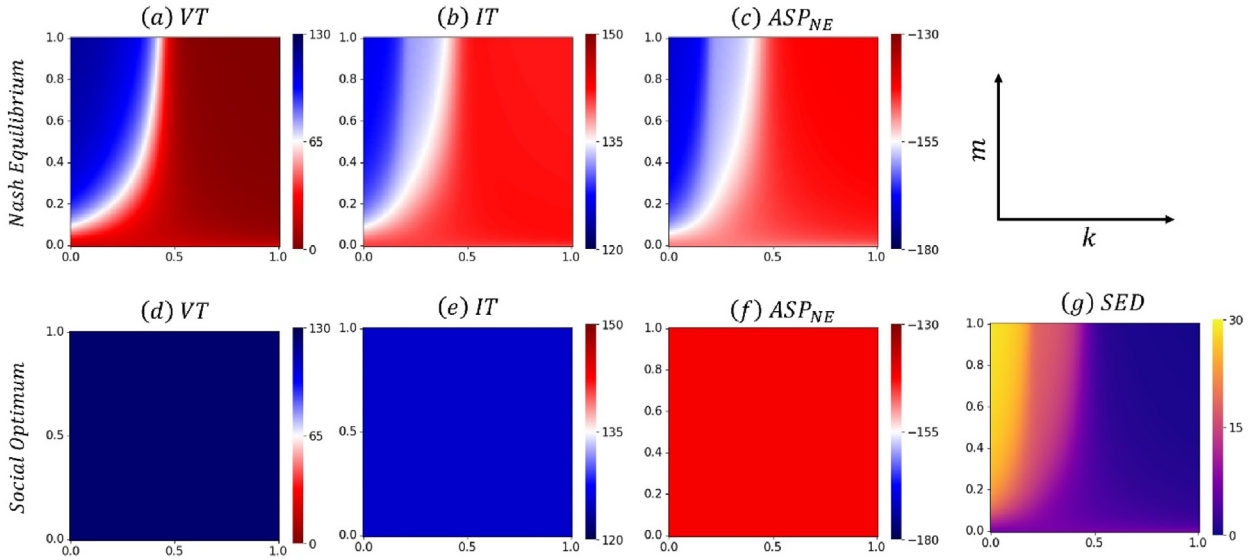

Fig. 10. The total number of vaccinated people, the total number of infected people, ASP, and SED. Panels (a) – (c) are for the NE case and panels (d) – (f) are for the SO case. Panel (g) represents the SED, which is the difference between panels (f) and (c). All the panels are drawn in terms of the relative sensitivity due to vaccination cost (k) along the $x-$ axis ranging from 0 to 1 and the inertial effect of vaccination rate (m) along the $y-$ axis both ranging from 0 to 1. The total number of vaccinated people is depicted with a range from 0 to 130, the total number of infected people is depicted with a range from 0 to 150, the ASPs are depicted with a range from – 180 to – 130 and the SED is depicted with a range from 0 to 30. The other parameters are the same as in the basic case. From the figures, we see that the social dilemma is monotonically increasing with the increase of m and decrease of k.

Panel (c) presents the Average Social Payoff (ASP), combining the outcomes from panels (a) and (b) with their associated costs. The ASP is depicted as not being particularly sensitive to the parameters m and k.

In the social optimum panels (d) – (e), vaccination remains at a maximum level, and infection remains at a minimum level. Given that the parameters m and k are not present in the equations for vaccination flow, the social optimum suggests that both vaccination and infection should incur minimum costs. Panel (f), representing the average social payoff, also exhibits low sensitivity to the parameters m and k.

The difference between panel (f) and panel (c) is represented in panel (g), depicting the Social SED. In the SED panel, a monotonic increase in the dilemma is observed with an increase in the inertial effect (m) and a decrease in the sensitivity parameter (k). This illustrates that a higher inertial effect and lower sensitivity lead to an escalation of the social dilemma.

4. Conclusion

The dynamics of infectious diseases and the vaccination process are invariably shaped by individual behaviors. In the context of multistrain infectious diseases such as seasonal influenza and COVID-19, the decision-making process is predominantly contingent upon factors such as the cost and efficacy of available vaccinations. Furthermore, the rate of waning immunity constitutes a crucial determinant in the selection of vaccinations.

In the context of epidemic models, each individual is initially regarded as susceptible and possesses the freedom to opt for any available vaccination. The initial selection is contingent upon factors such as the overall count of infected individuals, as well as the cost and efficacy of the vaccinations. Typically, individuals tend to opt for vaccinations with lower costs. Given the inherent imperfections in vaccinations, individuals experience a gradual decline in immunity over time. Consequently, the phenomenon of waning immunity also exerts a notable influence on the selection of vaccinations, particularly in consideration of their long-term efficacy.

Some previous studies also studied these kinds of models. Epidemic models with multiple vaccination options considering cost and efficacy were mentioned in (Rajib Arefin et al., 2019). The vaccination behavior of humans and the waning immunity effect in epidemic models were also analyzed in (Buonomo, 2020; Kabir, 2021; Khan et al., 2022a, 2023; Wu, Zhang, Song, & Xia, 2024; Zuo et al., 2022a, 2022b). Some analytic and numerical simulations concerning the multistrain epidemic model were presented in (Khan et al., 2022a, 2023; Rajib Arefin et al., 2019). Human behavior towards vaccination involving cost and efficacy was studied in (Ariful Kabir et al., 2019; Kabir & Tanimoto, 2020; Khan et al., 2023; Rajib Arefin et al., 2019). However, no other studies were conducted concerning a multi-strain epidemic model considering two vaccination options in the presence of waning immunity and the cost-effectiveness of vaccinations.

In our current study, we employed behavior equations to scrutinize vaccination choices, considering the presence of multistrain dynamics. Through numerical simulations, we observed an initial preference among individuals for vaccines with lower costs and reduced efficacy. However, as the waning rate increased, there was a shift towards favoring vaccines with higher costs and efficacy. Notably, the presence of multistrain dynamics led to an earlier attainment of vaccine equilibrium.

Our subsequent investigation focused on vaccine dominance, revealing scenarios where both vaccines could dominate within specific parameter ranges. Additionally, we identified instances of co-existence, where both vaccines were chosen equally. The analysis of equilibrium highlighted that increasing the efficacy ratio between two vaccines diminished certain dominance patterns.

Furthermore, our examination delved into the social dilemma inherent in the model. We computed average social payoffs at equilibrium, encompassing costs associated with infection and vaccination. A comparison was made with socially optimum average social payoffs, determined by considering a time-constant vaccination rate for both vaccines. Discrepancies between these two payoffs elucidated the social efficiency deficit, explaining the social dilemma inherent in the model. Our findings indicated that escalating waning immunity rates and transmission rates heightened the social dilemma. Regarding vaccination costs, the dilemma reached its maximum when both vaccination costs were at their peak. Moreover, the social dilemma was exacerbated when the sensitivity constant related to vaccination cost was minimized, and the inertial effect of vaccination rate was maximized.

Our exploration of vaccination behavior, vaccine dominance, and the social dilemma was conducted using a simple ordinary differential equation model (mean-field approximation). The inclusion of a social context in our data lends credibility to our results. In future investigations, we plan to employ a multiagent simulation approach to further analyze and validate these findings.

Funding

Funding was received for this work.

Intellectual property

We confirm that we have given due consideration to the protection of intellectual property associated with this work and that there are no impediments to publication, including the timing of publication, concerning intellectual property. In so doing we confirm that we have followed the regulations of our institutions concerning intellectual property.

Research ethics

We further confirm that any aspect of the work covered in this manuscript that has involved human patients has been conducted with the ethical approval of all relevant bodies and that such approvals are acknowledged within the manuscript.

IRB approval was obtained (required for studies and series of 3 or more cases).

Written consent to publish potentially identifying information, such as details of the case and photographs, was obtained from the patient(s) or their legal guardian(s).

Authorship

The International Committee of Medical Journal Editors (ICMJE) recommends that authorship be based on the following four criteria:

1. Substantial contributions to the conception or design of the work; or the acquisition, analysis, or interpretation of data for the work; AND
2. Drafting the work or revising it critically for important intellectual content; AND
3. Final approval of the version to be published; AND

Agreement to be accountable for all aspects of the work in ensuring that questions related to the accuracy or integrity of any part of the work are appropriately investigated and resolved.

All those designated as authors should meet all four criteria for authorship, and all who meet the four criteria should be identified as authors. For more information on authorship, please see http://www.icmje.org/recommendations/browse/roles-and-responsibilities/defining-the-role-of-authors-and-contributors.html.

All listed authors meet the ICMJE criteria. We attest that all authors contributed significantly to the creation of this manuscript, each having fulfilled the criteria as established by the ICMJE.

We confirm that the manuscript has been read and approved by all named authors.

We confirm that the order of authors listed in the manuscript has been approved by all named authors.

Contact with the editorial office

This author submitted this manuscript using his/her account in EVISE.

We understand that this Corresponding Author is the sole contact for the Editorial process (including EVISE and direct communications with the office). He/she is responsible for communicating with the other authors about progress, submissions of revisions, and final approval of proofs.

We confirm that the email address shown below is accessible by the Corresponding Author, is the address to which the Corresponding Author's EVISE account is linked, and has been configured to accept email from the editorial office of the American Journal of Ophthalmology Case Reports.

CRediT authorship contribution statement

Md. Mamun-Ur-Rashid Khan: Writing – review & editing, Writing – original draft, Visualization, Software, Methodology, Investigation, Formal analysis, Conceptualization. **Jun Tanimoto:** Writing – review & editing, Writing – original draft, Supervision, Project administration, Funding acquisition, Formal analysis, Conceptualization.

Declaration of competing interest

No conflict of interest exists.

Acknowledgements

This study received financial support in the form of a Grant-in-Aid for Scientific Research from the Japan Society for the Promotion of Science (JSPS), specifically through KAKENHI (Grant No. JP 23H03499). The funding, allocated to Professor Tanimoto, played a crucial role in facilitating various aspects of this research. We express our sincere gratitude to JSPS for their support and acknowledge their contribution to the successful completion of this study.

References

Arefin, M. R., Kabir, K. M. A., Jusup, M., Ito, H., & Tanimoto, J. (2020). Social efficiency deficit deciphers social dilemmas. *Scientific Reports, 10*, 1–9. https://doi.org/10.1038/s41598-020-72971-y

Ariful Kabir, K. M., Jusup, M., & Tanimoto, J. (2019). Behavioral incentives in a vaccination-dilemma setting with optional treatment. *Physics Reviews E., 100*, 1–13. https://doi.org/10.1103/PhysRevE.100.062402

Bauch, C. T. (2005). Imitation dynamics predict vaccinating behaviour. *Proceedings of the Royal Society B Biological Sciences, 272*, 1669–1675. https://doi.org/10.1098/rspb.2005.3153
Buonomo, B. (2020). Effects of information-dependent vaccination behavior on coronavirus outbreak : Insights from a SIRI model. *Ricerche di Matematica, 69*, 483–499. https://doi.org/10.1007/s11587-020-00506-8
Cabrera, M., Córdova-Lepe, F., Gutiérrez-Jara, J. P., & Vogt-Geisse, K. (2021). An SIR-type epidemiological model that integrates social distancing as a dynamic law based on point prevalence and socio-behavioral factors. *Scientific Reports, 11*, 1–16. https://doi.org/10.1038/s41598-021-89492-x
Chun-Miin Chen, A. C. S. (2021). Simulating influenza epidemics with waning vaccine immunity. *Medicine (Baltimore)*. https://doi.org/10.1097/MD.0000000000027169
Dong, S., Xu, L., Ding, Z. L., & Bo, X. (2023). Application of a time-delay SIR model with vaccination in COVID-19 prediction and its optimal control strategy. *Nonlinear Dynamics, 111*, 10677–10692. https://doi.org/10.1007/s11071-023-08308-x
Fahdilla, C., Putri, A. R., & Haripamyu, H. (2021). Bifurcation analysis of epidemic model waning immunity. *Journal of Physics: Conference Series, 1940*, Article 012014. https://doi.org/10.1088/1742-6596/1940/1/012014
Fenichela, E. P., Castillo-Chavezb, C., Ceddiac, M. G., Chowellb, G., Gonzalez Parrae, P. A., Hickling, G. J., et al. (2011). Adaptive human behavior in epidemiological models. *Proceedings of the National Academy of Sciences of the United States of America, 108*, 6306–6311. https://doi.org/10.1073/pnas.1011250108
Hamami, D., Cameron, R., Pollock, K. G., & Shankland, C. (2017). Waning immunity is associated with periodic large outbreaks of mumps: A mathematical modeling study of scottish data. *Frontiers in Physiology, 8*, 1–11. https://doi.org/10.3389/fphys.2017.00233
Kabir, K. M. A. (2021). How evolutionary game could solve the human vaccine dilemma. *Chaos, Solitons & Fractals, 152*, Article 111459. https://doi.org/10.1016/j.chaos.2021.111459
Kabir, K. M. A., Kuga, K., & Tanimoto, J. (2019a). Analysis of SIR epidemic model with information spreading of awareness. *Chaos, Solitons & Fractals, 119*, 118–125. https://doi.org/10.1016/j.chaos.2018.12.017
Kabir, K. M. A., Kuga, K., & Tanimoto, J. (2019b). Effect of information spreading to suppress the disease contagion on the epidemic vaccination game. *Chaos, Solitons and Fractals, 119*, 180–187. https://doi.org/10.1016/j.chaos.2018.12.023
Kabir, K. A., Kuga, K., & Tanimoto, J. (2020). The impact of information spreading on epidemic vaccination game dynamics in a heterogeneous complex network- A theoretical approach. *Chaos, Solitons & Fractals, 132*, Article 109548. https://doi.org/10.1016/j.chaos.2019.109548
Kabir, K. M. A., Ovi, M. A., Murtyas, S., Hagishima, A., & Tanimoto, J. (2023). Acceptance and willingness-to-pay of vaccine for COVID-19 in Asian Countries: A hypothetical assessment survey. *Evergreen, 10*, 617–625. https://doi.org/10.5109/6792807
Kabir, K. M. A., Risa, T., & Tanimoto, J. (2021). Prosocial behavior of wearing a mask during an epidemic: An evolutionary explanation. *Scientific Reports, 11*, 1–14. https://doi.org/10.1038/s41598-021-92094-2
Kabir, K. M. A., & Tanimoto, J. (2019). Analysis of epidemic outbreaks in two-layer networks with different structures for information spreading and disease diffusion. *Communications in Nonlinear Science and Numerical Simulation, 72*, 565–574. https://doi.org/10.1016/j.cnsns.2019.01.020
Kabir, K. M. A., & Tanimoto, J. (2020). Cost-efficiency analysis of voluntary vaccination against n -serovar diseases using antibody-dependent enhancement : A game approach. *Journal of Theoretical Biology, 503*, Article 110379. https://doi.org/10.1016/j.jtbi.2020.110379
Kermack, W. O., & McKendrick, A. G. (1927). A contribution to the mathematical theory of epidemics. *Royal Society A: Mathematical, Physical & Engineering Sciences, 115*, 700–721. https://doi.org/10.1098/rspa.1927.0118
Khalaf, S. L., & Flayyih, H. S. (2023). Analysis , predicting , and controlling the COVID-19 pandemic in Iraq through SIR model. *Results Control Optim, 10*, Article 100214. https://doi.org/10.1016/j.rico.2023.100214
Khan, M. M. U. R., Arefin, M. R., & Tanimoto, J. (2022a). Investigating vaccination behavior and disease dynamics of a time-delayed two-strain epidemic model: An evolutionary approach. *International Exchange and Innovation Conference on Engineering and Sciences*, 147–154. https://doi.org/10.5109/5909084
Khan, M. M.-U.-R., Arefin, M. R., & Tanimoto, J. (2022b). Investigating the trade-off between self-quarantine and forced quarantine provisions to control an epidemic: An evolutionary approach. *Applied Mathematics and Computation, 432*, Article 127365. https://doi.org/10.1016/j.amc.2022.127365
Khan, M. M.-U.-R., Arefin, M. R., & Tanimoto, J. (2023). Time delay of the appearance of a new strain can affect vaccination behavior and disease dynamics: An evolutionary explanation. *Infectious Disease Modelling, 8*, 656–671. https://doi.org/10.1016/j.idm.2023.06.001
Khan, M. M.-U.-R., & Tanimoto, J. (2023). Investigating the social dilemma of an epidemic model with provaccination and antivaccination groups : An evolutionary approach. *Alexandria Engineering Journal, 75*, 341–349. https://doi.org/10.1016/j.aej.2023.05.091
Kuga, K., & Tanimoto, J. (2018). Which is more effective for suppressing an infectious disease: Imperfect vaccination or defense against contagion? *Journal of Statistical Mechanics: Theory and Experiment, 2018*, Article 23407. https://doi.org/10.1088/1742-5468/aaac3c
Kumar, M., & Abbas, S. (2022). Age-structured SIR model for the spread of infectious diseases through indirect contacts. *Mediterranean Journal of Mathematics, 19*, 1–18. https://doi.org/10.1007/s00009-021-01925-z
Markovič, R., Šterk, M., Marhl, M., Perc, M., & Gosak, M. (2021). Socio-demographic and health factors drive the epidemic progression and should guide vaccination strategies for best COVID-19 containment. *Results in Physics, 26*. https://doi.org/10.1016/j.rinp.2021.104433
Nakata, Y., & Omori, R. (2015). Delay equation formulation for an epidemic model with waning immunity: An application to mycoplasma pneumoniae. *IFAC-PapersOnLine, 28*, 132–135. https://doi.org/10.1016/j.ifacol.2015.11.024
Nana-kyere, S., Boateng, F. A., Jonathan, P., Donkor, A., Hoggar, G. K., Titus, B. D., et al. (2022). Global analysis and optimal control model of COVID-19. *Computational and Mathematical Methods in Medicine, 2022*. https://doi.org/10.1155/2022/9491847
Nishimura, I., Arefin, R., Tatsukawa, Y., & Utsumi, S. (2023). Social dilemma analysis on vaccination game accounting for the effect of immunity waning. *Chaos, Solitons & Fractals, 171*, Article 113426. https://doi.org/10.1016/j.chaos.2023.113426
Rajib Arefin, M., Masaki, T., Ariful Kabir, K. M., & Tanimoto, J. (2019). Interplay between cost and effectiveness in influenza vaccine uptake: A vaccination game approach. *Royal Society A: Mathematical, Physical & Engineering Sciences, 475*. https://doi.org/10.1098/rspa.2019.0608
Tanimoto, J. (2015). *Fundamentals of evolutionary game theory and its applications*. Tokyo: Springer.
Tanimoto, J. (2021). *Sociophysics approach to epidemics*. Tokyo: Springer.
Tatsukawa, Y., Arefin, R., Tanaka, M., & Tanimoto, J. (2021). Free ticket , discount ticket or intermediate of the best of two worlds — which subsidy policy is socially optimal to suppress the disease spreading. *Journal of Theoretical Biology, 520*, Article 110682. https://doi.org/10.1016/j.jtbi.2021.110682
Tatsukawa, Y., Arefin, M. R., Utsumi, S., & Tanimoto, J. (2022). Investigating the efficiency of dynamic vaccination by consolidating detecting errors and vaccine efficacy. *Scientific Reports, 12*, 1–12. https://doi.org/10.1038/s41598-022-12039-1
Tori, R., & Tanimoto, J. (2022). A study on prosocial behavior of wearing a mask and self-quarantining to prevent the spread of diseases underpinned by evolutionary game theory. *Chaos, Solitons and Fractals, 158*, Article 112030. https://doi.org/10.1016/j.chaos.2022.112030
Turkyilmazoglu, M. (2021). Explicit formulae for the peak time of an epidemic from the SIR model. *Physica D: Nonlinear Phenomena, 422*, Article 132902. https://doi.org/10.1016/j.physd.2021.132902
Turkyilmazoglu, M. (2022a). A restricted epidemic SIR model with elementary solutions. *Physica A: Statistical Mechanics and its Applications, 600*, Article 127570. https://doi.org/10.1016/j.physa.2022.127570
Turkyilmazoglu, M. (2022b). An extended epidemic model with vaccination: Weak-immune SIRVI. *Physica A: Statistical Mechanics and its Applications, 598*, Article 127429. https://doi.org/10.1016/j.physa.2022.127429
Tyson, R. C., Hamilton, S. D., Lo, A. S., Baumgaertner, B. O., & Krone, S. M. (2020). The timing and nature of behavioural responses affect the course of an epidemic. *Bulletin of Mathematical Biology, 82*, 1–28. https://doi.org/10.1007/s11538-019-00684-z
Utsumi, S., Arefin, M. R., Tatsukawa, Y., & Tanimoto, J. (2022). How and to what extent does the anti-social behavior of violating self-quarantine measures increase the spread of disease? *Chaos, Solitons & Fractals, 159*. https://doi.org/10.1016/j.chaos.2022.112178

Van Boven, M., De Melker, H. E., Schellekens, J. F. P., & Kretzschmar, M. (2000). Waning immunity and sub-clinical infection in an epidemic model: Implications for pertussis in The Netherlands. *Mathematical Biosciences, 164*, 161–182. https://doi.org/10.1016/S0025-5564(00)00009-2

Wang, F., Liu, M., Zhang, L., & Xie, B. (2023). Bifurcation analysis and optimal control of a network- based SIR model with the impact of medical resources. *Nonlinear Analysis Modelling and Control, 28*, 209–227. https://doi.org/10.15388/namc.2023.28.30770

Webb, G. (2021). A COVID-19 epidemic model predicting the effectiveness of vaccination in the US. *Infectious Disease Reports, 13*, 654–667. https://doi.org/10.3390/IDR13030062

Wei, Y., Lin, Y., & Wu, B. (2019). Vaccination dilemma on an evolving social network. *Journal of Theoretical Biology, 483*. https://doi.org/10.1016/j.jtbi.2019.08.009

Wu, Z. (2021). Social distancing is a social dilemma game played by every individual against his/her population. *PLoS One, 16*, 1–26. https://doi.org/10.1371/journal.pone.0255543

Wu, Y., Zhang, Z., Song, L., & Xia, C. (2024). Global stability analysis of two strains epidemic model with imperfect vaccination and immunity waning in a complex network. *Chaos, Solitons & Fractals, 179*, Article 114414. https://doi.org/10.1016/j.chaos.2023.114414

Zuo, C., Zhu, F., & Ling, Y. (2022). Analyzing COVID-19 vaccination behavior using an SEIRM/V epidemic model with awareness decay. *Frontiers in Public Health, 10*, 1–12. https://doi.org/10.3389/fpubh.2022.817749

Zuo, C., Zhu, F., Meng, Z., Ling, Y., Zheng, Y., & Zhao, X. (2022). Analyzing the COVID-19 vaccination behavior based on epidemic model with awareness-information. *Infection, Genetics and Evolution, 98*, Article 105218. https://doi.org/10.1016/j.meegid.2022.105218